Thiophene-rich fused-aromatic thienopyrazine acceptor for donor–acceptor low band-gap polymers for OTFT and polymer solar cell applications†

Rajib Mondal,[a] Hector A. Becerril,[a] Eric Verploegen,[ad] Dongwook Kim,‡[b] Joseph E. Norton,[b] Sangwon Ko,[a] Nobuyuki Miyaki,[a] Sangjun Lee,[c] Michael F. Toney,[d] Jean-Luc Brédas,[b] Michael D. McGehee[c] and Zhenan Bao*[a]

Received 31st March 2010, Accepted 22nd April 2010
First published as an Advance Article on the web 4th June 2010
DOI: 10.1039/c0jm00903b

Thiophene enriched fused-aromatic thieno[3,4-*b*]pyrazine systems were designed and employed to produce low band gap polymers (E_g = 1.0–1.4 eV) when copolymerized with fluorene and cyclopentadithiophene. The copolymers are mainly investigated for organic thin film transistor and organic photovoltaic applications. Molecular packing in the thin films of these polymers was investigated using Grazing incidence X-ray Scattering. Although both fluorene and cyclopentadithiophene polymers follow similar face to face π–π stacking, the latter polymers show much smaller lamellar d-spacings due to side-chain interdigitation between the lamellae. This lead to the higher charge carrier mobilities in cyclopentadithiophene polymers (up to 0.044 cm2/V.s) compared to fluorene polymers (up to 8.1×10^{-3} cm^2/V.s). Power conversion efficiency of 1.4% was achieved using fluorene copolymer in solar cells with a fullerene derivative as an acceptor. Although the cyclopentadithiophene polymers show lower band gaps with higher absorption coefficients compared to fluorene copolymers, but the power conversion efficiencies in solar cells of these polymers are low due to their low ionization potentials.

1. Introduction

Development of new polymer semiconducting materials has become an active area of research in recent years due to their potential uses in light weight and flexible organic photovoltaics (OPVs) and organic thin-film transistors (OTFTs).[1–5] However, in many instances, the lower efficiency and limited air stability of polymers has limited their commercial use.[1] A combination of donor polymer and fullerene derivative (as acceptor) is commonly used in bulk heterojunction (BHJ) solar cells. In most of these solar cells, a small region of the solar spectrum is absorbed, mainly in the visible region. For example, poly-(phenylene vinylene) (PPV)[6] and poly(3-hexyl thiophene) (P3HT)[7] have band gaps larger than 1.9 eV, and thus absorb only 30% from the AM1.5 (air mass) solar photon flux. Lower band gap polymers can achieve absorption of a greater fraction of light from the solar spectrum and enable a higher efficiency solar cell.[8] In addition, it is important for the polymer to have good charge-carrier mobility for efficient charge dissociation.[9]

Recently, we have reported electron-deficient fused aromatic thienopyrazine (**TP**) units for donor–acceptor type conjugated polymers.[10,11] The fused **TP** unit provides a planar and electron rich π-face that enhances π–π stacking between the polymeric chains.[12,13] It was shown that a field-effect mobility as high as 0.2 cm^2/Vs can be achieved using acenaphthylthienopyrazine type copolymers.[10] However, the power conversion efficiency (PCE) was limited to only 1.4% for BHJs with the polymers in this class, which may be due to higher band gaps (~1.65 eV) and lower absorption coefficients ($3–6 \times 10^4$ cm^{-1}).[11] Interestingly, the band-gap can be significantly lowered by replacing acenaphthyl with phenanthrene in the **TP** unit. However, the absorption coefficient in the latter polymer became rather low (3.4×10^4 cm^{-1}) and the charge carrier mobility was also reduced. We conjectured that the lower mobility could be due to lower molecular weight of the phenanthrene-based polymer,[14] which was again limited by poor solubility. This was also responsible for the poor device performance.

In this study, we describe the design and synthesis of fused **TP** units enriched with thiophene groups in the form of benzodithiophene (**BDT**) – the dithiophene analog of phenanthrene. Detailed quantum-chemical characterization was carried out using density functional theory (DFT). Thiophene-rich fused aromatic units in conjugated polymers are of particular importance due to in general their lower reorganization energies and improved device performance compared to the corresponding benzene analogs.[15] Thiophene derivatives are also well known to provide better solubility in organic solvents compared to their benzene analogs. Copolymers of these thiophene enriched fused-aromatic **TP** with fluorene (**FL**)

[a]*Department of Chemical Engineering, Stanford University, Stanford, CA, 94305. E-mail: zbao@stanford.edu*
[b]*School of Chemistry and Biochemistry and Center for Organic Photonics and Electronics, Georgia Institute of Technology, Atlanta, GA, 30332*
[c]*Department of Materials Science, Stanford University, Stanford, CA, 94305*
[d]*Stanford Synchrotron Radiation Lightsource, Menlo Park, CA, 94025*

† Electronic supplementary information (ESI) available: Transistor and solar cell fabrication, HOMO and LUMO wavefunctions of the monomers, absorption spectra of the polymers in solution and thin films, *I–V* and output curves of *p*-type OTFTs of **BDTup-FL** and **BDTup-CPDT**. See DOI: 10.1039/c0jm00903b

‡ Current address: Department of Chemistry, Kyonggi University, Suwon, 443-760, Korea

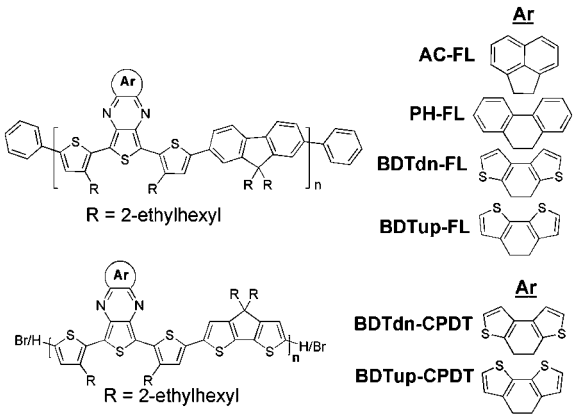

Chart 1 Structures of the thienopyrazine copolymers containing fused aromatic units discussed in this work. Synthesis and device performances of **AC-FL** and **PH-FL** were previously reported.[11]

and cyclopentadithiophene (**CPDT**) derivatives (Chart 1) are synthesized. 3-(2-Ethylhexyl)thiophene groups were introduced to both sides of a fused aromatic **TP** to enhance the solubility in common organic solvents. 2-Ethylhexyl groups (branched alkyl chains) were chosen for this study as this class of polymers with branched alkyl chains have shown better efficiency in BHJ solar cells compared to the ones with linear alkyl chains.[11] The synthesized polymers were used to fabricate OTFT and BHJ solar cell devices and the performance of these devices is discussed. Packing in the thin film was investigated using Grazing incidence X-ray Scattering. The observed differences in device performance appear to be related to variations in interchain π–π interactions and lamellar d-spacing. The **CPDT** polymers show lower band gaps, higher absorption coefficients, and higher charge-carrier mobility compared to the **FL** copolymers; they also form smoother thin films. However, the **FL** copolymers present higher power conversion efficiencies in solar cells.

2. Experimental

Synthesis of monomers

2,5-Bis(3-(2-ethylhexyl)thiophen-2-yl)-3,4-dinitrothiophene (3). 3-(2-Ethylhexyl)-2-tributylstannylthiophene (**1**) and 2,5-dibromo-3,4-dinitrothiophene (**2**) were synthesized following literature reported procedures. Compounds **1** (5.4 g, 12 mmol), **2** (2.0 g, 6 mmol), and catalytic amount $PdCl_2(PPh_3)_2$ (44 mg, 0.06 mmol) were placed in dry 35 mL microwave proof thick walled glass vial equipped with a stir bar and a snap cap. 20 mL of dry THF was added and degassed by bubbling Ar gas for 30 min. The solution was heated at 70 °C using 200 W of microwave power for 2 h. After the reaction, THF was evaporated in a rotary evaporator and the oily product was subjected to column chromatography (silica gel, 20% CH_2Cl_2 in hexane). The compound **3** was isolated yellow viscous liquid (3.3 g, 98%). ^{1}H NMR (300 MHz, $CDCl_3$) δ 0.8 (m, 12 H), 1.193 (m, 16 H), 1.52 (m, 2H), 2.517 (d, J = 7.2 Hz, 4 H), 6.988 (d, J = 5.1 Hz, 2 H), 7.482 (d, J = 5.1 Hz, 2 H); HRMS (EI) m/z = 563.2070 (M + H$^+$), calcd m/z = 563.2067.

2,5-Bis(3-(2-ethylhexyl)thiophen-2-yl)thiophene-3,4-diamine (4). Compound **3** (1.15 g, 2.04 mmol) was dissolved in 35 mL of ethanol and 35 mL of conc. HCl was added carefully. The reaction mixture was cooled to 0 °C and a solution of stannous chloride dihydrate (17.5 g, 77 mmol) in 25 mL ethanol was added slowly. The resulted reaction mixture was vigorously stirred at 30 °C for overnight (~18 h). The reaction mixture was poured into 50 mL of cold 25% sodium hydroxide solution. The resulted basic solution was passed through a tightly packed celite pad, followed by washing with toluene. The aqueous layer was extracted with toluene. Drying in a rotary evaporator under reduced pressure yielded 1.02 g (100%) of diamine **4**. ^{1}H NMR (300 MHz, $CDCl_3$) δ 0.8 (m, 12 H), 1.2 (m, 16 H), 1.604 (m, 2H), 2.536 (d, J = 7.2 Hz, 4 H), 3.436 (s, 4H), 6.940 (d, J = 5.4 Hz, 2 H), 7.280 (d, J = 5.1 Hz, 2 H).

Benzo[1,2-*b*:4,3-*b*′]dithiophene-4,5-dione (5). 3,3′-Bithiophene (10 g, 60 mmol) was taken in a dry 500 mL round bottom flask and 175 mL of dry 1,2-dichloroethane was added. Three portions of oxalyl chloride (3 mL, 34.5 mmol) were added in each 5 days and the reaction mixture was continuously refluxed for 15 days under Ar atmosphere. The reaction mixture was cooled to rt and then kept in refrigerator for overnight. The resulted red precipitate was filtered and washed with hexanes and warm ethanol. Yield of dione **5** was 10.1g (76%). ^{1}H NMR (300 MHz, $CDCl_3$) δ 7.282 (d, J = 7.8 Hz, 2 H), 7.818 (d, J = 7.8 Hz, 2 H); HRMS (EI) m/z = 220.9726 (M + H$^+$), calcd m/z = 220.9726.

Benzo[2,1-*b*:3,4-*b*′]dithiophene-4,5-dione (6). 50 mL of ethanol and 12 mL of water were added to 2,2′-bithiophene-3,3′-dicarboxaldehyde (1.2 g, 5.4 mmol). Sodium cyanide (0.1 g, 2 mmol) was added to the reaction mixture and refluxed for 2 h. The reaction flask was then cooled slowly and kept under ambient condition for overnight to promote aerial oxidation of the reaction mixture. The resulted black precipitate (0.3 mg) was filtered out and washed with hexane and ethanol. The filtrate was extracted with CH_2Cl_2, the solvent was dried with Na_2SO_4; and evaporated in a rotary evaporator. The crude redish product was subjected to column chromatography (silica gel, 50% CH_2Cl_2 in hexanes) to yield another 0.15 g of dione **6**. The overall yield was 0.45 g (38%). ^{1}H NMR (300 MHz, $CDCl_3$) δ 7.206 (d, J = 5.1 Hz, 2 H), 7.498 (d, J = 5.1 Hz, 2 H); HRMS (EI) m/z = 220.9722 (M + H$^+$), calcd m/z = 220.9726.

8,10-Bis(3-(2-ethylhexyl)thiophen-2-yl)trithieno[3,4-*b*:2′,3′-*f*:3″,2″-*h*]quinoxaline (7). Diamine **4** (0.99 g, 1.97 mmol) and dione **5** (0.42 g, 1.90 mmol) were suspended in 75 mL of dry chloroform. Catalytic amount of *p*-toluenesulfonic acid (38 mg, 0.2 mmol) was added. The pH of the solution should be little acidic at this stage. The resulted solution was stirred overnight under Ar atm to yield a deep green solution. The chloroform solution was washed with dil. $NaHCO_3$ (aq.) and dried using anhydrous Na_2SO_4. After removing the solvent in rotary evaporator, the crude product was subjected to column chromatography (silica gel, 25% CH_2Cl_2 in hexanes) to yield compound **7** as green powder (0.77 g, 57%). ^{1}H NMR (300 MHz, $CDCl_3$) δ 0.820 (m, 12 H), 1.2–1.4(m, 16 H), 1.78 (m, 2H), 3.002 (d, J = 7.5 Hz, 4 H), 7.042(d, J = 5.1 Hz, 2 H), 7.459(d, J = 5.1 Hz, 2 H), 7.63(d, J = 5.1 Hz, 2 H), 7.73(d, J = 5.1 Hz, 2 H); ^{13}C NMR (125 MHz, $CDCl_3$) δ 11.696, 15.086, 24.063, 26.792, 29.685, 33.613, 35.825, 40.558, 124.275, 124.615, 127.633, 130.166, 131.200, 131.725,

136.878, 137.864, 139.327, 140.677, 140.930; HRMS (EI) m/z = 687.2021 (M + H^+), calcd m/z = 687.2024.

8,10-Bis(3-(2-ethylhexyl)thiophen-2-yl)trithieno[3,4-*b*:3′,2′-*f*:2″,3″-*h*]quinoxaline (8). Compound **8** was synthesized from dimaine **4** and dione **6** similarly as described for the synthesis of compound **7**. Yield = 78%. ^{1}H NMR (400 MHz, $CDCl_3$) δ 0.822 (m, 12 H), 1.2–1.38 (m, 16 H), 1.812 (m, 2H), 3.004 (d, J = 7.6 Hz, 4 H), 7.036 (d, J = 5.2 Hz, 2 H), 7.423(d, J = 5.2 Hz, 2 H), 7.444 (d, J = 5.2 Hz, 2 H), 8.279 (d, J = 5.2 Hz, 2 H); ^{13}C NMR (100 MHz, $CDCl_3$) δ 11.692, 15.089, 24.068, 26.790, 29.687, 33.607, 35.860, 40.576, 124.599,125.160, 126.738, 127.451, 130.241, 131.151, 136.406, 137.036, 139.425, 140.729, 140.888; HRMS (EI) m/z = 687.2018 (M + H^+), calcd m/z = 687.2024.

8,10-Bis(5-bromo-3-(2-ethylhexyl)thiophen-2-yl)trithieno[3,4-*b*:2′,3′-*f*:3″,2″-*h*]quinoxaline (9). *N*-Bromosuccinimide (0.302 g, 1.7 mmol) in 25 mL of DMF was added dropwise to a suspension of the compound **7** (0.53 g, 0.77 mmol) in 50 mL of DMF at −20 °C for 30min. The reaction mixture was stirred for 2h at −20 °C, warmed to room temperature. The resulted solution was poured into water and extracted with CH_2Cl_2. The crude product was then subjected to column chromatography (silica gel, 15% CH_2Cl_2 in hexanes). Yield = 0.3 g, 46%. ^{1}H NMR (300 MHz, $CDCl_3$) δ 0.850 (m, 12 H), 1.2–1.4(m, 16 H), 1.77 (m, 2H), 2.91 (d, J = 7.5 Hz, 4 H), 6.98(s, 2 H), 7.645(d, J = 5.1 Hz, 2 H), 7.751(d, J = 5.1 Hz, 2 H); ^{13}C NMR (125 MHz, $CDCl_3$) δ 11.692, 15.142, 24.087, 26.7, 29.641, 33.453, 36.294, 40.233, 115.434, 123.137, 124.130, 131.941, 132.298, 133.051, 136.441, 137.852, 138.594, 140.124, 140.261; HRMS (EI) m/z = 843.0249 (M + H^+), calcd m/z = 843.0235.

8,10-Bis(5-bromo-3-(2-ethylhexyl)thiophen-2-yl)trithieno[3,4-*b*:3′,2′-*f*:2″,3″-*h*]quinoxaline (10). *N*-Bromosuccinimide (0.230 g, 1.3 mmol) in 30 mL of DMF was added dropwise to a suspension of the compound **8** (0.4 g, 0.59 mmol) in 15 mL of DMF at −20 °C for 30min. The reaction mixture was stirred for 2h at −20 °C, warmed to room temperature. After stirring the reaction mixture for overnight, the resulted solution was extracted with chloroform and washed with water. Finally, the crude product was subjected to column chromatography (silica gel, 15% CH_2Cl_2 in hexanes). Yield = 49%. ^{1}H NMR (400 MHz, $CDCl_3$) δ 0.890 (m, 12 H), 1.2–1.43 (m, 16 H), 1.77 (m, 2H), 2.757 (d, J = 7.2 Hz, 4 H), 6.809 (s, 2 H), 7.276 (d, J = 5.2 Hz, 2 H), 7.921 (d, J = 5.2 Hz, 2 H); ^{13}C NMR (100 MHz, $CDCl_3$) δ 11.692, 15.172, 24.113, 26.707, 29.657, 33.456, 36.413, 40.159, 115.272, 123.022, 125.100, 126.518, 132.410, 132.835, 135.754, 136.907, 138.371, 139.713, 139.993; HRMS (EI?) m/z = 845.0199 (M + H^+), calcd m/z = 845.0214.

General procedure for Suzuki polycondensation reaction. 0.5 mL of potassium carbonate solution (aq., 2M) was added to a mixture of compound **9** or **10** (0.1 mmol), 2,7-bis-(trimethyleneborate)-9,9-bis(2-ethylhexyl)fluorene (**11**, 0.1 mmol), tetrakis(triphenylphosphine)palladium (0) (3.5 mg, 3 mol%), and Aliquat®336 (0.02 g) in 2 mL of *o*-dichlorobenzene under argon. The reaction mixture was frozen and degassed under vacuum for three times. Then the reaction mixture was heated to 95 °C and stirred for 5 days. These polymers were end capped with phenyl group by adding excess of phenylboronic acid and bromobenzene. Crude polymers were precipitated in methanol and washed with hexane and acetone. These polymers were further redissolved in 5 mL of chloroform along with Pd(0) scavenger[16] and stirred at rt for overnight. The solution filtered through a 0.45 μm PTFE syringe filter and precipitated in methanol. The polymer was filtered and washed with acetone and hexane.

BDTdn-FL: Yield = 90%, GPC (THF): M_w = 12844, M_n = 7510, PDI = 1.71; ^{1}H-NMR (300MHz, $CDCl_3$) δ 0.5–1.5 (m, 58 H), 1.9–2.1 (m, 6H), 3.1 (br, 4H), 7.34 (br, 4H), 7.6–7.9 (m, 8H); anal. calcd for $C_{67}H_{80}N_2S_5$: C 74.95, H 7.51, N 2.61, S 14.93; found C 73.53, H 6.92, N 2.39, S 13.87. **BDTup-FL**: Yield = 92%, GPC (THF): M_w = 33783, M_n = 12895, PDI = 2.62; ^{1}H-NMR (300MHz, $CDCl_3$) δ 0.5–1.5 (m, 58 H), 1.85–2.15 (m, 6H), 3.15 (br, 4H), 7.35 (br, 4H), 7.76 (br, 6H), 8.7 (br, 2H); anal. calcd for $C_{67}H_{80}N_2S_5$: C 74.95, H 7.51, N 2.61, S 14.93; found C 74.14, H 7.33, N 2.41, S 13.91.

General procedure for microwave assisted Stille polycondensation reaction. Compound **9** or **10** (84.5 mg, 1 mmol), 4,4-bis(2-ethylhexyl)-2,6-bis(trimethylstannyl)-4H-cyclopenta[2,1-*b*:3,4-*b*′]dithiophene (**12**, 1 mmol) and catalytic amount tetrakis(triphenylphosphine)palladium(0) (5 mg, 4.3 mol%) were placed in dry 7 mL microwave proof thick walled glass vial equipped with a stir bar and a snap cap. 2 mL of dry toluene was added and degassed by bubbling Ar gas for 30 min. The solution was heated using fixed power (300 W) for 1 h. Maximum temperature of 180 °C and internal pressure of 30 PSI reached during the reaction. The polymer was precipitated in methanol. 1 mL of conc. HCl was added. The crude polymer was filtered and washed with acetone and hexanes. Polymers were further purified as described for the Suzuki polycondensation reaction.

BDTdn-CPDT: Yield = 85%, GPC (THF): M_w = 13702, M_n = 8620, PDI = 1.59; ^{1}H-NMR (300MHz, $CDCl_3$) δ 0.6–1.5 (m, 58 H), 1.8–2.2 (m, 6H), 3.05 (br, 4H), 7.15–7.3 (m, 4H), 7.5–7.8 (m, 4H); anal. calcd for $C_{63}H_{76}N_2S_7$: C 69.69, H 7.06, N 2.58, S 20.67; found C 67.69, H 6.60, N 2.48, S 19.24; **BDTup-CPDT**: Yield = 89%, GPC (THF): M_w = 17250, M_n = 10150, PDI = 1.70; ^{1}H-NMR (300MHz, $CDCl_3$) δ 0.6–1.5 (m, 58 H), 1.8–2.1 (m, 6H), 3.0 (br, 4H), 6.9–7.3 (m, 4H), 7.48 (br, 2H), 8.4 (b, 2H); anal. calcd for $C_{63}H_{76}N_2S_7$: C 69.69, H 7.06, N 2.58, S 20.67; found C 69.42, H 6.88, N 2.51, S 19.32.

3. Results and discussion

3.1 Synthesis of monomers and polymers

2,5-Bis(3-(2-ethylhexyl)thiophen-2-yl)thiophene-3,4-diamine (**4**) was synthesized almost quantitatively by reducing 2,5-bis(3-(2-ethylhexyl)thiophen-2-yl)-3,4-dinitrothiophene (**3**) using $SnCl_2$/HCl in ethanol (Scheme 1).[17] Dinitro compound **3** was prepared following a microwave assisted Stille coupling reaction between

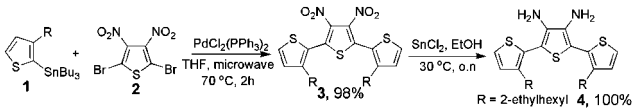

Scheme 1

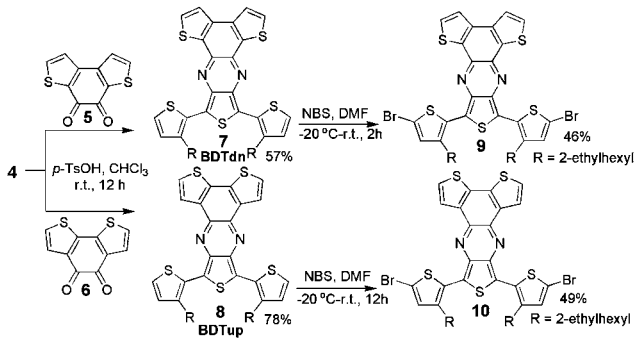

Scheme 2

two equivalent of 3-(2-ethylhexyl)-2-tributylstannylthiophene (**1**) and one equivalent of 2,5-dibromo-3,4-dinitrothiophene (**2**). Condensation between diamine **4** and benzo[1,2-b:4,3-b′]dithiophene-4,5-dione (**5**) and benzo[2,1-b:3,4-b′]dithiophene-4,5-dione (**6**) in chloroform yielded fused aromatic TPs; 8,10-bis(3-(2-ethylhexyl)thiophen-2-yl)trithieno[3,4-b:2′,3′-f:3″,2″-h]quinoxaline (BDTdn, **7**; 57%) and 8,10-bis(3-(2-ethylhexyl)thiophen-2-yl)trithieno[3,4-b:3′,2′-f:2″,3″-h]quinoxaline (BDTup, **8**; 78%), respectively. Quinone **5** was synthesized with 76% yield by a reported Friedel–Crafts acylation reaction of 3,3′-bithiophene with oxalyl chloride.[18] Synthesis of quinone **6** was achieved by a intramolecular benzoin condensation of 2,-2′-bithiophene-3,3′-dicarboxaldehyde with 38% yield.[19] Bromination of **7** and **8** with N-bromosuccinimide (NBS) in DMF afforded 8,10-bis(5-bromo-3-(2-ethylhexyl)thiophen-2-yl)trithieno[3,4-b:2′,3′-f:3″,2″-h]quinoxaline (**9**, 46%) and 8,10-bis(5-bromo-3-(2-ethylhexyl)thiophen-2-yl)trithieno[3,4-b:3′,2′-f:2″,3″-h]quinoxaline (**10**, 49%), respectively (Scheme 2).[11] These compounds contain the bromo polymerizable sites that were used for the polymerization. They are also relatively stable and readily soluble in chlorinated organic solvents.

Donor–acceptor type copolymers of these fused **TPs** with fluorene (**FL**) and cyclopentadithiophene (**CPDT**)[15,20] were synthesized *via* Suzuki and Stille polycondensation reactions, respectively (Scheme 3). The **TP** units are electron poor and act as acceptor units, whereas **FL** and **CPDT** are donor units in the polymer chain. The Suzuki coupling between **9** and **10** with 2,7-bis(trimethyleneborate)-9,9-bis(2-ethylhexyl)fluorene (**11**) yielded **FL** copolymers **BDTdn-FL** and **BDTup-FL**, respectively, with good yields.[21,22] These polymers were end-capped with phenyl groups. When toluene was used as solvent for polymerization reactions, the molecular weights (M_w) of the polymers were very low. We assumed that the lower solubility of the polymers in toluene was responsible for low Mw. Polymerization

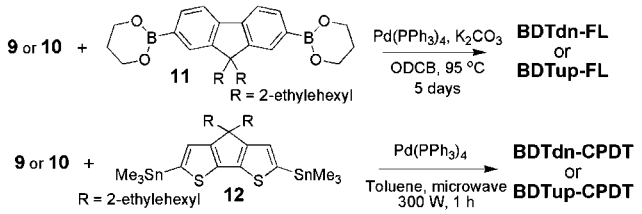

Scheme 3

in *o*-dichlorobenzene (ODCB) afforded relatively higher M_w polymers, since conjugated polymers are usually more soluble in chlorinated solvents and higher temperature can be used for polymerization due to the higher boiling point of ODCB. For example, the number average molecular weight (M_n) of **BDTup-FL** was increased to 13000 g/mol from 6000 g/mol by changing the solvent from toluene to ODCB for polymerization.

Microwave assisted Stille coupling reactions were carried out between **9** and **10** with 4,4-bis(2-ethylhexyl)-2,6-bis(trimethylstannyl)-4H-cyclopenta[2,1-*b*:3,4-*b*′]dithiophene (**12**) in toluene to synthesize the **CPDT** copolymers **BDTdn-CPDT** and **BDTup-CPDT**, respectively. Any tin complex remaining in these polymers were hydrolyzed with dilute HCl in MeOH to yield bromo or hydrogen end-capped polymers. Microwave assisted polymerization has advantages over the traditional thermal polymerization reactions.[23] High M_w polymers can be synthesized within a very short time period using microwave. It is believed that decomposition of any reactive intermediates are minimized by the very fast microwave-assisted heating. In our case, we carried out the polymerization for one hour. M_ws are increased during the successive irradiation in the first 20–30 mins, as observed during the optimization processes. A relatively low M_w polymer was synthesized following the traditional thermal polymerization reaction, even though the reaction was carried out for more than 5 days. The Suzuki coupling reaction could not be optimized as it uses a heterogeneous aqueous reaction mixture and the solution boils vigorously under microwave radiation.

After both Suzuki and Stille coupling reactions, polymers were precipitated from the reaction mixtures into MeOH. The precipitate was filtered and redissolved in chloroform with palladium scavenger in order to remove any residual palladium catalyst.[24] Precipitation in methanol followed by filtration and washing with acetone and hexane afforded pure polymers. These polymers are soluble in hot tetrahydrofuran (THF), chloroform, chlorobenzene, and ODCB.

3.2 Optical and electrochemical properties

The optical and electrochemical properties of the polymers were investigated in ODCB and in thin films and are summarized in Table 1. The absorption spectra of the thin films of the **FL** copolymers (**BDTdn-FL** and **BDTup-FL**) are compared with acenaphthyl- and phenanthrene-based **FL** copolymers[11] in Fig. 1. The absorption peaks are mainly located in two regions; around 300–500 nm and around 525–775 nm for acenaphthyl and 600–950 nm for the others. The absorption spectra of the **BDT**-based **FL** copolymers are very similar to those of the phenanthrene-based **FL** copolymers with significant absorption in the near-infrared region of the solar spectrum. This can help in generating higher photocurrent in photovoltaic devices by absorbing more sunlight. The fused aromatic unit used for **TP** strongly affects the band gap of the resulting polymer. It was shown that the band gap or the absorption edge could be efficiently reduced by more than 0.2 eV by changing the aromatic unit from acenaphthyl to phenanthrene.[11] Band gaps can be further reduced by ~0.1 eV by introducing **BDT** units, the thiophene analogs of phenanthrene. However, no dramatic changes in the absorption coefficients were observed. Absorption coefficients are in the range of

Table 1 Optical and Electrochemical Properties of the Polymers

		Solution (in *o*-dichlorobenzene)				Thin Films				
Polymers	M_w (PDI)[a]	A_{max}(nm)	HOMO[b](V)	LUMO[b](V)	Eg(eV)	A_{max}(onset)(nm)	$\alpha(cm^{-1})$ [d]	E_g(eV)[c]	HOMO[e](V)	LUMO[e](V)
PH-FL	7710 (1.57)	445, 730	−4.85	−3.45	1.40 1.41[c]	464, 742 (888)	3.4×10^4	1.40	−4.93	−3.53
BDTdn-FL	12844 (1.71)	349, 447, 774	−4.85	−3.52	1.33 1.29[c]	329, 447, 777 (964)	3.0×10^4	1.29	−5.16	−3.87
BDTup-FL	33783 (2.62)	336, 393, 746	−4.84	−3.45	1.39 1.32[c]	349, 357, 779 (955)	3.5×10^4	1.30	−5.00	−3.70
BDTdn-CPDT	13702 (1.59)	368, 515, 893	−4.60	−3.53	1.07 1.11[c]	368, 505, 904(1204)	4.0×10^4	1.03	-	-
BDTup-CPDT	17250 (1.70)	354, 499, 839	−4.60	−3.46	1.14 1.14[c]	356, 509, 870 (1117)	6.2×10^4	1.11	-	-

[a] Determined from GPC using the THF soluble part using polystyrene as standard and THF as eluent, Weight average molecular weight (M_w) in Daltons, and PDI = Polydispersity index. [b] Measured from cyclic voltammetry in *o*-dichlorobenzene and calibrated based on the oxidation potential of Fc/Fc^+. [c] Estimated from the onset of the absorption spectra. [d] ($O.D._{max} \times$ ln10)/thickness of the film. [e] HOMO energy levels were estimated from PES.

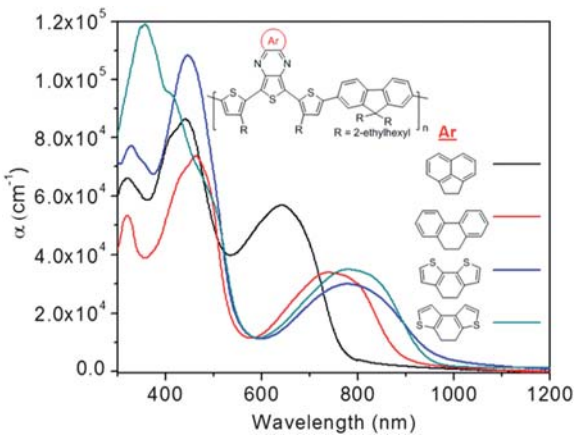

Fig. 1 Absorption spectra of the thin films of acenaphthyl, phenanthrene, and benzodithiophene-based **FL** copolymers. The general structure of the polymers is given in the inset.

3–3.5 $\times$ 10^4 cm^{-1} in the thin films of **BDT** and phenanthrene-based **FL** copolymers.

The electronic properties of the monomer units and oligomer structures of the **BDT** copolymers were calculated (as isolated molecules) at the Density Functional Theory (DFT) B3LYP/6-31G(d,p) level. The frontier energy levels (HOMO and LUMO) were characterized for the neutral electronic states. The vertical and adiabatic ionization potentials (IP) and electron affinities (EA) were computed using the neutral and ionic potential energy surfaces, and the lowest singlet excited state transitions were calculated using Time Dependent (TD) DFT methods (Table S3). The properties of the polymers were extrapolated from oligomer calculations and Kuhn fits of energy versus 1/N where N is the number of formal double bonds in the molecule.[25] Note that the calculations were performed on model systems of **BDT** copolymers where all side-chain substituents were replaced with methyl groups (this has only minimal effect on the electronic properties).

The calculated HOMO levels among the fluorene-containing copolymers (**AC-FL**, **PH-FL**, **BDTdn-FL**, and **BDTup-FL**) display similar characteristic and have energies within a narrow range of −4.3–−4.4 eV (Table 6). The LUMO levels are more affected by the nature of the electron-accepting group and exhibit a larger energy variation ranging from −2.50 eV for **AC-FL** to −2.83 eV for **BDTdn-FL**. The lowest-energy LUMOs and corresponding smaller HOMO–LUMO gap energies (which we denote here as E_g) occur in the systems containing BDT groups. The E_g values extrapolated for **BDTdn-FL** and **BDTup-FL** are 1.51 and 1.59 eV, respectively, and are as much as 0.4 eV lower than that of the **AC-FL** copolymer and 0.1 to 0.2 eV lower than that of the **PH-FL** copolymer. A similar effect is observed from the calculated IP, EA, and transition energies, where the S_1 transition energies of the **BDT** polymers are noticeably lower than those of the **AC-FL** and **PH-FL** polymers; the S_1 transition energy (optical gap) for the **BDTdn-FL** polymer is calculated to be 1.24 eV.

The differences in the electronic energy levels calculated for the copolymers are attributed to shifts in the LUMO levels originating from the nature of the aromatic group fused onto the electron-accepting moieties. The HOMO and LUMO wavefunctions of the **PH-FL** and **BDT** copolymers are shown in Fig. 2. For each copolymer, the LUMO wavefunction localizes onto the fused aromatic groups and thus is more affected by the electron-accepting nature of the acceptor, while the HOMO wavefunction is more delocalized along the polymer backbone and only marginally affected by the acceptor characteristics. The thiophene-enriched **BDT** groups enhance the electron-accepting nature of the thienopyrazine group of the acceptor.

The HOMO (ionization potential) and LUMO (electron affinity) energies were determined from cyclic voltammetry, performed under argon atmosphere with a supporting electrolyte of 0.05 M n-Bu_4NPF_6 in anhydrous ODCB. The HOMO of the **CPDT** copolymers (4.6 eV) is located higher than in the **FL** copolymers (~4.85 eV) in solution. However, the LUMO energy of both the **FL** or **CPDT** copolymers remains constant, since they share the same electron-accepting units. For example, the LUMO energy of both **BDTdn-FL** and **BDTdn-CPDT** polymer is ~3.52 eV. The ionization potentials (IPs) of the polymer films were measured by photoelectron spectroscopy (PES). IPs of **BDTdn-FL** and **BDTup-FL** are 5.16 and 5.0 eV, respectively. The

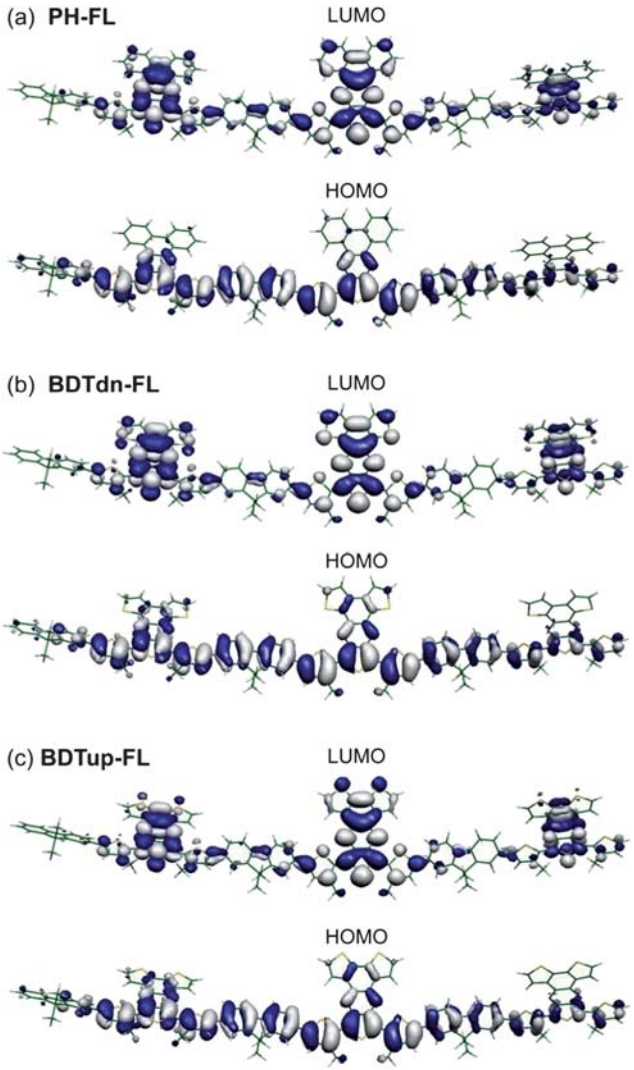

Fig. 2 HOMO and LUMO wavefunctions of the (a) **PH-FL**, (b) **BDTdn-FL**, and (c) **BDTup-FL** oligomer (n = 3) model systems calculated at the B3LYP/6-31G(d,p) level of theory.

PES measurement in air becomes erroneous for **CPDT** copolymers; this is probably due to oxygen doping[25] in the polymer films with lower IPs. In the present instance, the LUMO energies in the thin films can be estimated from the HOMO energies and optical band gap of the polymer films (λ_{onset} of the absorption spectra); that the optical band gaps can be used for this purpose is due to the fact that the electrochemical band gaps ($E_g = E_{LUMO} - E_{HOMO}$) are very similar with the optical band gaps determined from solution. For the **PH-FL** and the **BDT** copolymers in solution and in thin films, the trends observed from the experimental E_g and optical gap values reported in Table 1 are supported by the calculation results. In agreement with the calculations, the experimental E_g values for the **BDT** copolymers are also ~0.1 eV lower than those of the **PH-FL** copolymer.

Absorption coefficients (α) are significantly enhanced by copolymerizing these **BDT** monomers with **CPDT** units. For example, α is increased by almost a factor of two from the **FL** copolymer **BDTup-FL** (3.5×10^4 cm^{-1}) to the **CPDT** copolymer **BDTup-CPDT** (6.2×10^4 cm^{-1}), Fig. 3. Absorption of **CPDT** copolymers (**BDTdn-CPDT** and **BDTup-CPDT**) becomes relatively broader compared to **FL** copolymers (**BDTdn-FL** and **BDTup-FL**) and extends up to 1210 and 1125 nm with band gaps of 1.03 and 1.11 eV for polymers **BDTdn-CPDT** and **BDTup-CPDT**, respectively.

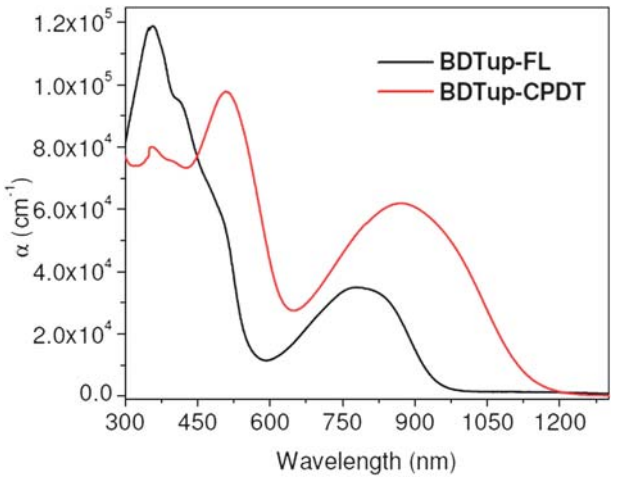

Fig. 3 Absorption spectra of the thin films of **BDTup-FL** and **BDTup-CPDT**.

Comparing the polymer absorption of thin films and in solution, the **BDTdn** copolymers are red shifted by only 5–10 nm, whereas the **BDTup** copolymers are red-shifted by ~30 nm. This suggests stronger intermolecular interactions and hence tighter inter-chain packing for **BDTup** polymers compared to **BDTdn** polymers (*vide infra*). Absorption coefficients of the **BDTup** copolymers are also 1.2–1.5 times higher compared to **BDTdn** copolymers due to tighter inter-chain packing.

3.3 Thermal properties and molecular packing

The thermal properties of the polymers were investigated by thermogravimetric analysis (TGA) and differential scanning calorimetry (DSC). All of these polymers showed thermal decomposition temperature in the range of 400–420 °C under nitrogen by TGA, indicating good thermal stability. No thermal transition signals were observed from 0 °C to 350 °C in the DSC for these four polymers. DSC signals could be observed only for the polymers in this class that are substituted with linear alkyl chains;[11] polymers with branched alkyl chains usually do not show any DSC peaks due to poor ordering.

Grazing incidence X-ray Scattering (GIXS) was employed to investigate crystallinity and packing of the benzodithiophene-based polymers. The data are summarized in Table 2 and room

Table 2 d-spacing and π–π stacking distances of the **BDTdn-FL**, **BDTup-FL**, **BDTdn-CPDT**, and **BDTup-CPDT**

Polymer	d-spacing/layer-layer spacing (Å)	π–π stacking (Å)	X
BDTdn-FL	19.9	4.39	
BDTup-FL	22.6	3.85	
BDTdn-CPDT	12.8	4.05	
BDTup-CPDT	13.7	4.01	

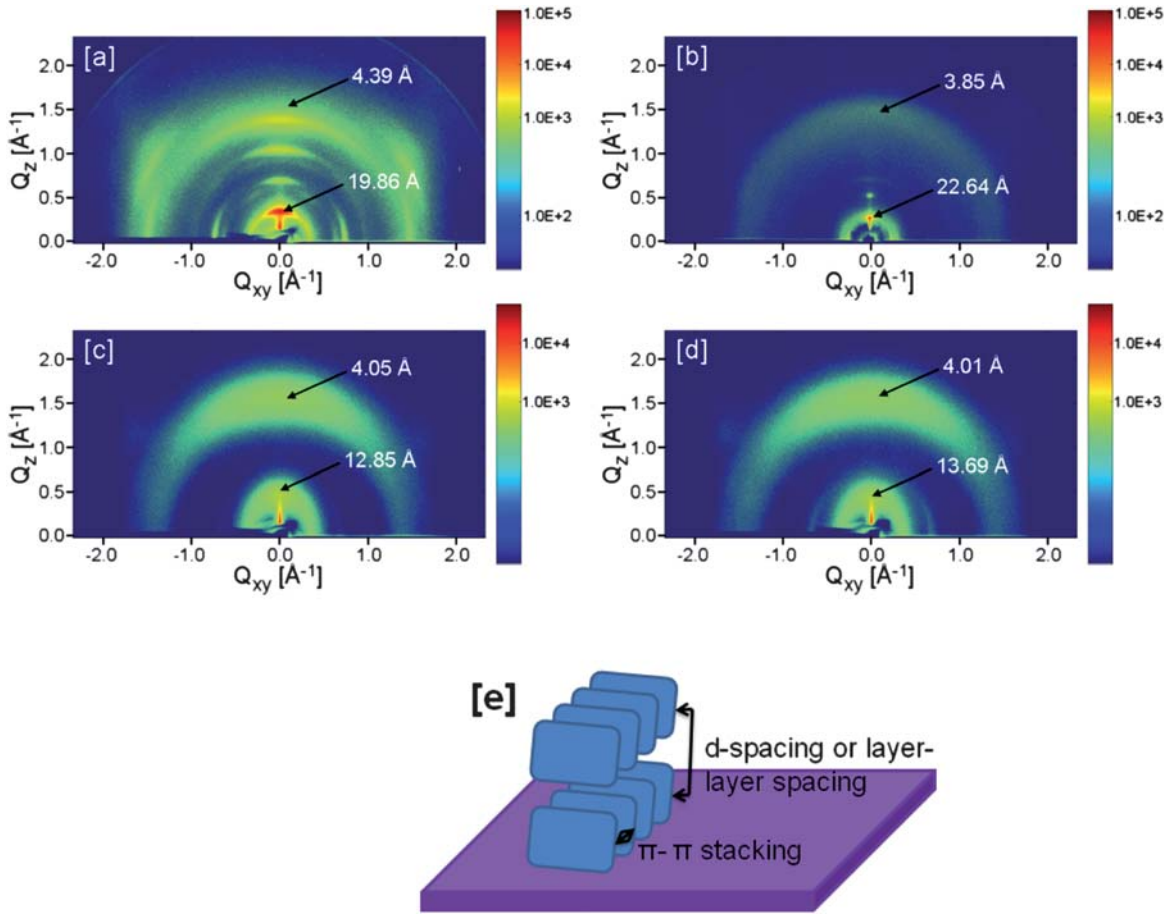

Fig. 4 GIXS images of polymer films (a) **BDTdn-FL**, (b) **BDTup-FL**, (c) **BDTdn-CPDT**, and (d) **BDTup-CPDT**. (e) Cartoon representing d-spacing and π–π stacking distances.

temperature GIXS images of polymer films spin casted on bare silicon (in situ annealing temperature ~200 °C) are shown in Fig. 4. The sulfur atoms in the benzodithiophene unit face towards the polymer main chain in **BDTdn-FL** and **BDTdn-CPDT**, while they point away from the polymer main chain in **BDTup-FL** and **BDTup-CPDT**. In addition, alkyl side chains on the donor units and the fused aromatic rings are very likely on the same side for the **CPDT** copolymers while they are expected to point in opposite directions in the **FL** copolymers. These structural differences have a marked impact on the film morphology of the **FL** copolymers while their influence in the **CPDT** copolymers appears to be only marginal; we found differences on the order of 2.7 Å and more than 0.5 Å in lamellar d-spacing and π–π stacking distances for **FL** copolymers, respectively, while for the **CPDT** copolymers the lamellar d-spacings differ by less than 1 Å and the π–π stacking distances are nearly equal.

With regards to interlayer d(100) lamellar spacings, they are significantly smaller in **CPDT** copolymers (12.8~13.7 Å) than in **FL** copolymers (19.9~22.6 Å). This is likely due to interdigitation of the side chains in the **CPDT** copolymers (vide infra). It is also apparent from the images shown in Fig. 4 that the **BDTdn-FL** polymer has better order than the other polymers. The other polymers have only two or three broad reflections, showing that they are poorly ordered. It is interesting to note that the film texture (crystallographic orientation) of all these polymers is different than the usual (100) orientation. The GIXS images in Fig. 4 show that the π–π stacking direction is nominally oriented normal to the substrate surface and the (100) reflections predominate in the substrate plane. We suspect that this is due to the two dimensional like structure of the polymers.

In order to shed some light on the nature of the interchain packing in these polymers, four possible dimer forms of each donor–acceptor monomer unit were optimized (Fig. 5) with the

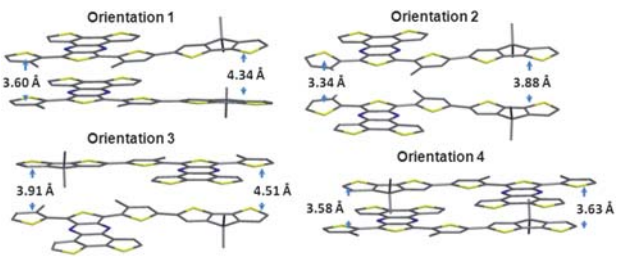

Fig. 5 Four different orientations of **BDTup-CPDT** obtained from DFTB calculations (tilt view, see Figure S1 for additional views); similar orientations of the monomer units were considered for **BDTdn-FL**, **BDTup-FL**, and **BDTdn-CPDT**. Note that for orientations 1 and 3, accepting units are on the same side while for orientations 2 and 4, they are pointing in opposite directions.

Density Functional Tight Binding (DFTB) methodology,[26,27] which is a semi-empirical type of approach able to describe well intermolecular interactions. Note that in these calculations all the long alkyl side chains are replaced with methyl groups; this simplification is justified by the fact that we are mainly interested here in evaluating the π–π interactions between the monomers, to which the longer alkyl chains contribute little (the long alkyl chains are, however, expected to impact significantly the interlayer d-spacings, see below). In all cases, the orientations involving antiparallel configurations between the fused **TP** units (orientation 2, Fig. 5) are calculated to be the most stable.

The calculations and GIXD data concur in providing very similar packing structures for **BDTdn-CPDT** and **BDTup-CPDT**. For the **FL** polymers the calculations suggest similar orientations (orientation 2) with similar π–π stacking distances for **BDTdn-FL** and **BDTup-FL**. However, the experimental results are very different. The interchain interactions in type-2 orientations between **CPDT** units (π–π distance ~3.9 Å) are stronger than those between of **FL** units (π–π distance ~4.7 Å). Thus, it is possible that packing of the **CPDT** polymers is dominated mainly by the interchain **CPDT** interactions irrespective of the nature of acceptor units including the position of the sulfur atoms in the fused **TP** units. In addition, the effects of side alkyl chains are practically the same for both polymers. However, due to the weaker interactions between the **FL** units, the positions of the sulfur atoms in the **TP** units and the side chains might play a more significant role in the thin-film packing of **BDTdn-FL** and **BDTup-FL**, which could explain that these polymers follow very different packing schemes.

In order to shed some light on the origin of the interlayer d-spacings in the polymers, plausible packing structures were constructed on the basis of the type-2 orientations in Fig. 5, using monomer units including the full alkyl side chains, see Fig. 6. The DFTD results suggest that, in the case of the **CPDT** polymers, the alkyl chains on the thiophene rings can "open up" to accommodate in between them the alkyl chains of a **CPDT** unit on a neighboring polymer. For the **FL** polymers, on the other hand, given that all the alkyl side chains of the thiophene and **FL** units are located on the same side, the steric hindrance among these chains prevents the same type of interdigitation as in the **CPDT** polymers. This feature could provide the origin for the longer d-spacing in the **FL** polymers *vs.* the **CPDT** polymers. However, more work, including classical molecular dynamics simulations, is warranted to reach a more definitive picture.[28]

3.4 Field-effect transistor characterization

The mobility of charge carriers (holes) in semiconducting polymers determines their applicability to transistors and OPV devices. High charge-carrier mobilities can lead to increased on-currents and faster switching speeds in transistors, and to increased photocurrent and power conversion efficiency in solar cells. Top-contact organic thin-film field-effect transistors (OTFT) were fabricated to measure the field-effect mobilities of the polymers. Although the diode mobility is more pertinent for PV applications, FET mobilities usually tend to correlate well with diode mobilities.[29] Polymer solutions in ODCB were drop-cast on octadecyltrimethoxysilane (OTS)-treated, heavily-doped, n-type SiO_2 (300 nm)/Si wafers. The average thickness of these polymer films was ~30 nm. The thin films were annealed at different temperatures and gold electrodes (40 nm) were deposited through shadow masks. Electrical performance was tested under dry N_2 atmosphere (glovebox). The results from optimized OTFTs for each polymer are summarized in Table 3. Representative *I–V* characteristics of OTFT devices fabricated from **BDTdn-FL** are shown in Fig. 7.

All of these polymers showed *p*-channel transport (h^+) with mobilities in the range of 10^{-5} to 10^{-2} $cm^2/(Vs)$ with a moderate

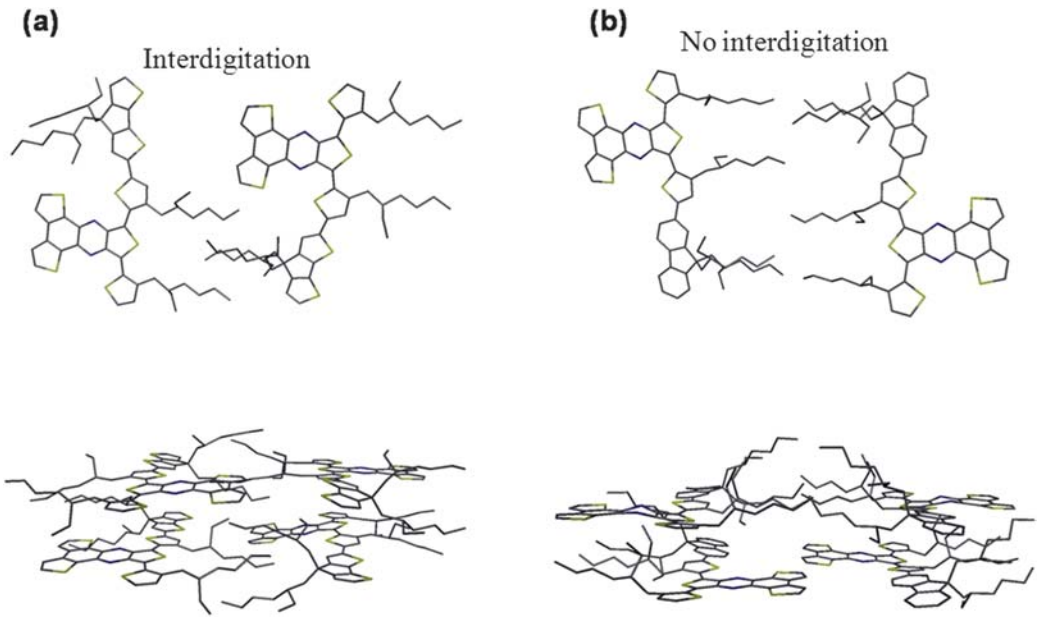

Fig. 6 Sketch of possible packing structures for (a) **CPDT** and (b) **FL** polymers; dimer configurations (top panel) and tetramer configurations (bottom panel).

Table 3 OTFT Characterization of the Polymers in N_2 environment.[a]

Polymer	μ_{max} cm^2/Vs	μ_{ave}* cm^2/Vs	$I_{on/off}$	V_{th} V
PH-FL	1.9×10^{-4}	1.6×10^{-4}	2.1×10^{3}	8.8
BDTdn-FL	1.6×10^{-5}	6.8×10^{-6}	64	17
BDTup-FL	8.1×10^{-3}	1.8×10^{-3}	3.53×10^{3}	−25
BDTdn-CPDT	3.1×10^{-4}	1.6×10^{-4}	1.7×10^{3}	−4
BDTup-CPDT	4.4×10^{-2}	3.8×10^{-3}	1.01×10^{3}	−13

[a] Average parameters extracted from at least 5 devices each. Mobilities reported are in the saturation regime. Top contact devices fabricated by drop-cast on octadecyltrimethoxysilane-treated SiO_2 (300 nm)/Si wafers. Device channel length was 50 μm and W/L = 20.

on/off ratio (in the order of 10^3) and low threshold voltages. A high hole carrier mobility of 0.2 $cm^2/(Vs)$ was obtained using the **FL** copolymer (**AC-FL**) with all linear alkyl chains.[10] The hole carrier mobility decreased to 0.07 $cm^2/(Vs)$ when linear alkyl chains were replaced by branched 2-ethylhexyl alkyl chains in the polymer.[11] This was rationalized based on differences between film morphology. Mainly, the polymer with linear alkyl chains was more crystalline than that with branched alkyl chains.[11] Compared to **AC-FL**, its phenanthrene analog **PH-FL** showed significantly reduced carrier mobility ($\mu_{max} \sim 10^{-4}$ $cm^2/(Vs)$) and its threshold voltage (V_{th}) for *p*-channel transport increases from 1.4 V to 8.8 V. Furthermore, replacing the aromatic unit by benzo[1,2-*b*:4,3-*b*′]dithiophene in polymer **BDTdn-FL** further reduces the carrier mobility ($\sim 10^{-5}$ $cm^2/(Vs)$) and V_{th} shifts to 17 V. This is consistent with the lower oxidation potential of the electron-rich phenanthrene- and benzodithiophene-type polymers. However, V_{th} (−23 V) shifts to a high negative voltage in the case of the benzo[2,1-*b*:3,4-*b*′]dithiophene-based polymer, **BDTup-FL**, and much higher carrier mobility ($\sim 10^{-2}$ $cm^2/(Vs)$) is achieved, which we attribute to the larger π–π stacking distance in **BDTdn-FL**. This leads to a small overlap between π orbitals on adjacent molecules and thus reduces the charge carrier mobility, despite the better order in this polymer compared to the others (see Fig. 4). In addition, **BDTdn-FL** produces a very rough film compared to **BDTup-FL** as indicated by AFM (Fig. 8).

The side chain interdigitation helps registration between the adjacent lamellae of **CPDT** polymers,[29] and is probably leading to high charge carrier mobilities compared to **FL** polymers. A hole carrier mobility of 0.044 cm^2/Vs is found for **BDTup-CPDT**. The mobility of **BDTdn-CPDT** is still lower and on the order of $\sim 10^{-4}$ cm^2/Vs. The thin film morphologies **CPDT** copolymers (**BDTdn-CPDT** and **BDTup-CPDT**) are also smoother compared to their **FL** analogs (**BDTdn-FL** and **BDTup-FL**) as indicated by the AFM images (Fig. 8).

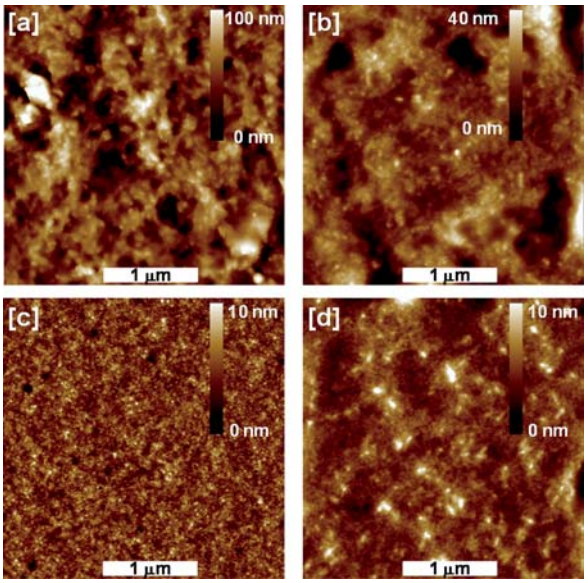

Fig. 8 Tapping mode AFM images of polymer films (a) **BDTdn-FL**, (b) **BDTup-FL**, (c) **BDTdn-CPDT**, and (d) **BDTup-CPDT**.

3.5 Photovoltaic characterization

Solar cell devices were fabricated using blends of each of these polymers and [6,6]-phenyl C_{61} butyric acid methyl ester

Table 4 Photovoltaic properties of the bulk heterojunction solar cells[a]

Polymer	J_{sc} mA/cm^2	V_{oc} V	FF	PCE %
PH-FL	2.3	0.48	0.52	0.57
BDTdn-FL	3.2	0.40	0.45	0.57
BDTup-FL	3.2	0.59	0.42	0.79
BDTdn-CPDT	0.64	0.375	0.60	0.14
BDTup-CPDT	3.1	0.345	0.37	0.40

[a] polymers/$PC_{61}BM$ (1 : 4) blend as active layer.

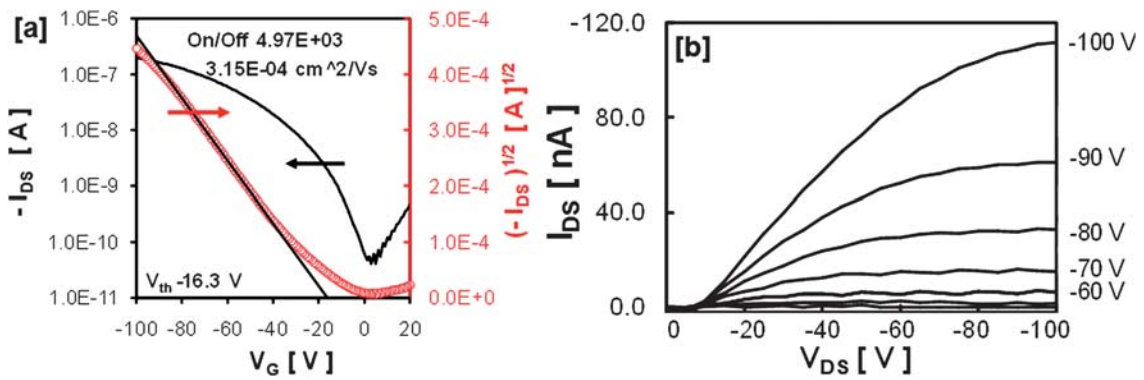

Fig. 7 Representative *I–V* and output curves of *p*-type OTFTs of **BDTdn-CPDT** (a, b) tested in the inert and dry atmosphere (glove box).

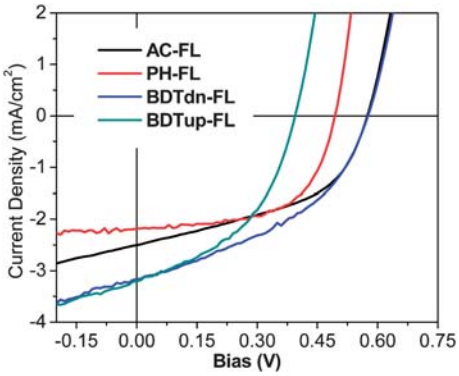

Fig. 9 *I–V* characteristics under AM1.5 illumination for the solar cell fabricated from **AC-FL**, **PH-FL**, **BDTdn-FL**, and **BDTup-FL** with PC[61]BM (1 : 4 weight ratio).

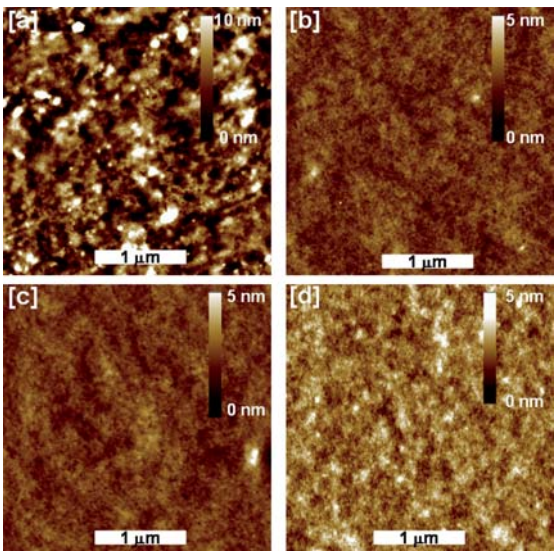

Fig. 10 Tapping mode AFM images of thin films of the blends of polymer and fullerene derivatives: (a) **BDTdn-FL** 1 : 1 with $PC_{61}BM$, (b) **BDTup-FL** 1 : 1 with $PC_{61}BM$, (c) **BDTup-FL** 1 : 4 with $PC_{61}BM$, and (d) **BDTup-FL** 1 : 1 with $PC_{71}BM$.

(PC[61]BM) with a device structure of ITO/PEDOT-PSS/polymer:PCBM/Al. Though several weight ratios of these polymers and PC[61]BM were tested, blends with a 1 : 4 ratio usually produced higher short-circuit current densities (J_{sc}), possibly due to formation of stable bimolecular structures of fullerene intercalated between the side-chains of the semiconducting polymer.[30] The solar cell data collected under simulated 1 sun AM 1.5G radiation are summarized in Table 4 and the representative *I–V* curves are shown in Fig. 9. The phenanthrene-based **FL** copolymer (**PH-FL**) was reported earlier[11] and its solar cell data are compared with the **BDT** copolymers. Polymer **BDTup-FL** shows the best power conversion efficiency (PCE) among these **FL** copolymers; this is likely due to its higher hole carrier mobility compared to **PH-FL** and **BDTdn-FL**. A slight increase in the V_{oc} was observed in **BDTup-FL** cells (~0.6 V) compared to **PH-FL** (~0.48 V) due to its higher ionization potential. Higher V_{oc} is expected in **BDTdn-FL** compared to **BDTup-FL** based on their HOMO energies. However, the V_{oc} (0.4 V) was significantly reduced in the case of the **BDTdn-FL** based solar cell, even though a similar J_{sc} was obtained (3.2 mA/cm^2). AFM of thin films of the blends indicates that **BDTdn-FL** tends to phase separate from PC[61]BM on long (100 nm) length scales (Fig. 10a). Since this is much longer than the exciton diffusion length, this contributes towards its poor performance. In addition, film quality of **BDTdn-FL**-based devices was bad due to its poor solubility in organic solvents. In contrast, **BDTup-FL** blends forms a very smooth films with PC[61]BM or with PC[71]BM irrespective of blending ratios (Fig. 10b–d), suggesting a much finer phase separation.

Solar cell efficiency of **BDTup-FL** was further optimized using different blending ratio of polymer with acceptor PC[61]BM and PC[71]BM (Table 5, Fig. 11). An optimized PCE of 1.38% (J_{sc} - 5.45 mA/cm^2, V_{oc} - 0.605 V, FF - 0.42) could be achieved using this polymer with PC[61]BM (1 : 3 blend ratio). Solar cell devices respond well in the visible to NIR region up to 980 nm, with a maximum external quantum efficiency of 14% at 750 nm and 30% at ~480 nm (Fig. 12). The previously reported **FL** copolymer without ring fusion showed maximum PCE of 2.2%.[31] For this copolymer, a higher J_{sc} (8.2 mA/cm^2) was achieved in optimized devices, while V_{oc} and FFs remain comparable to our devices made of **FL** copolymers, such as the **BDTup-FL** devices. Higher current is usually obtained by replacing PC[61]BM with PC[71]BM as an acceptor in the active layer, as the latter has higher absorption in the visible region.[32] However, the PCE could not be improved for **BDTup-FL** solar cells by using

Table 5 Optimization of PCE of solar cell containing **BDTup-FL**

Acceptor	Weight Ratio	Thickness (nm)	J_{sc} mA/cm^2	V_{oc} V	FF	PCE %
$PC_{61}BM$	1 : 1	100	4.38	0.625	0.35	0.96
	1 : 2	65	4.475	0.585	0.41	1.07
	1 : 3	85	5.45	0.605	0.42	1.38
	1 : 4	150	3.2	0.585	0.42	0.79
$PC_{71}BM$	1 : 1	62	3.7	0.575	0.39	0.83
	1 : 2	64	4.075	0.595	0.44	1.07
	1 : 3	87	4.625	0.585	0.43	1.16
	1 : 4	100	4.825	0.595	0.44	1.26

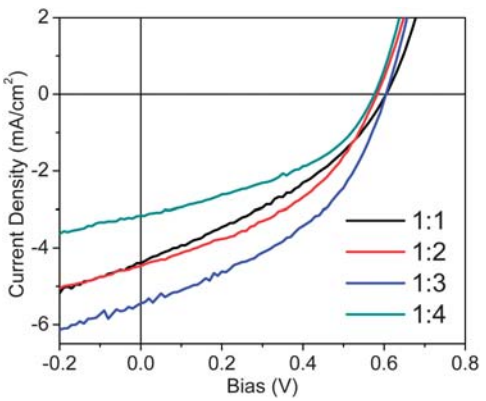

Fig. 11 *I–V* characteristics under AM1.5 illumination for the solar cell fabricated from **BDTup-FL** with different weight ratio of PC[61]BM (1 : 1, 1 : 2, 1 : 3, and 1 : 4).

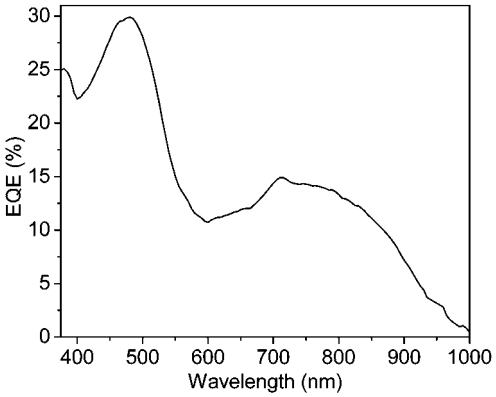

Fig. 12 EQE spectrum of a solar cell fabricated using blend of **BDTup-FL** and PC61BM (1 : 3 wt. ratio) in the active layer.

Table 6 B3LYP/6-31G(d,p) Energy Values of the Polymers Extrapolated from Oligomer Calculations.[a]

Compound	HOMO (V)[b]	LUMO (V)[b]	E_g (HOMO–LUMO) (eV)	IP (eV)[c]	EA (eV)[c]	S_1 (eV)[d]
AC-FL	−4.40	−2.50	1.90	4.86	−2.04	1.62
PH-FL	−4.42	−2.73	1.69	4.86	−2.27	1.41
BDTdn-FL	−4.34	−2.83	1.51	4.79	−2.37	1.24
BDTup-FL	−4.41	−2.82	1.59	4.86	−2.36	1.32

[a] Energies were extrapolated from Kuhn fits of oligomer (n = 1–3) calculations. [b] Gas-phase HOMO and LUMO levels. [c] Adiabatic values calculated from optimized structures on the neutral and ionic potential energy surfaces. [d] Vertical transition to the lowest S_1 state calculated at the TDDFT/B3LYP/6-31G(d,p) level.

a PC[71]BM acceptor; this may be due to morphological changes in **BDTup-FL**. A similar effect was observed in some other recently reported **TP** copolymers.[33]

Power conversion efficiencies of **CPDT** copolymers (0.14–0.40%) are low due to low open circuit voltages (0.35–0.38 V). As indicated earlier, ionization potentials of the **CPDT** polymers are lower compared to **FL** copolymers and thus reduce the V_{oc} and limit the efficiency. These **CPDT** polymers are among very few low band-gap polymers with band gap approaching 1 eV, some of which have been successfully used as donor material in the bulk heterojunction solar cell structure with fullerene derivatives as acceptor, but with very low PCE (<0.1%).[34]

We were able to achieve the desired low band gap for BHJ solar cells (<1.5 eV) and to induce a favorable packing of the donor–acceptor polymers by introducing novel fused aromatic units in the thienopyrazine structure as evidenced by the enhancement of charge carrier mobilities. Despite this achievement, low absorption coefficients (3–6.2 × 10^4 cm^{-1}) and high HOMO energies in these polymers limit their PCE. DFT calculations confirm that the electron density in the LUMO wave function is more localized on the acceptor fused **TP** unit of the polymers, while the electron density associated with the HOMO wave function is delocalized over both the acceptor and donor units (Fig. 3). The localization of the LUMO decreases orbital overlap with the HOMO, which can be detrimental to the strength of the lowest $S_0 \rightarrow S_1$ absorption. We have recently shown that the absence of the adjacent thiophenes around the acceptor enhances the HOMO/LUMO overlap and thus enhances the absorption coefficient for the lowest optical transition (which is dominated by HOMO-to-LUMO electron excitation).[35] This also raises the ionization potential. As a consequence, significant enhancement in PCE was observed in solar cell devices using the fused **TP** based polymer without adjacent thiophenes, due to increased open-circuit voltage and short-circuit current. Further investigation is underway to achieve higher efficiency solar cells.

4. Summary and conclusions

In summary, two isomers of benzodithiophene were fused into the aromatic thieno[3,4-*b*]pyrazine system and their fluorene copolymers are compared with the previously reported analogous polymers based on acenaphthyl and phenanthrene fused aromatic units. It can be concluded that introduction of fused aromatic units within thienopyrazine is a convenient approach to tune the optoelectronic properties of donor–acceptor polymers (E_g = 1.3 to 1.6 eV, HOMO = −4.9 to −5.2 V). We demonstrate that the improved π–π stacking afforded by the fused thienopyrazine units results in high hole mobilities (up to 0.2 cm^2/Vs). These polymers also show moderate power conversion efficiencies, up to 1.4% (**BDTup-FL** - Jsc = 5.45 mA/cm^2, Voc = 0.605 V, FF = 0.42), in bulk heterojunction devices. The band-gap of these fused thienopyrazine polymers could be further lowered by co-polymerizing with cyclopentadithiophene ($E_g \sim 1$ eV). Although both fluorene and cyclopentadithiophene polymers afford similar face-to-face π–π stacking cyclopentadithiophene polymers show higher charge carrier mobility (μFET = 0.044 cm^2/Vs) in thin film transistor devices compared to the analogous fluorene polymers (μFET = 8.1 × 10^{-3} cm^2/Vs). This result can be ascribed to decreased lamellar d-spacings of cyclopentadithiophene polymers as compared to the fluorene polymers yielding from side chain interdigitation between lamellae. However, the power conversion efficiencies of these cyclopentadithiophene polymers are limited due to low open circuit voltages caused by low ionization potentials. Maintaining all the properties of these cyclopentadithiophene polymers along with high ionization potential (>5.2 eV) will be necessary to achieve high efficiency solar cells.

Acknowledgements

This publication was partially based on work supported by the Center for Advanced Molecular Photovoltaics, Award No KUS-C1-015-21, made by King Abdullah University of Science and Technology (KAUST). We also acknowledge support from the Global Climate and Energy Program (GCEP) and the facility usage at the Stanford Center for Polymer Interfaces and Macromolecular Assemblies (CPIMA). Portions of this research were carried out at the Stanford Synchrotron Radiation Lightsource, a national user facility operated by Stanford University on behalf of the U.S. Department of Energy, Office of Basic Energy Sciences. R.M thanks Jack E. Parmer, George Margulis, and Eric Hoke for their help.

Notes and references

1 B. C. Thompson and J. M. J. Fréchet, *Angew. Chem. Int. Ed.*, 2008, **47**, 58–77.
2 N. S. Sariciftci, L. Smilowitz, A. J. Heeger and F. Wudl, *Science*, 1992, **258**, 1474–1476.
3 G. Yu, J. Gao, J. C. Hummelen, F. Wudl and A. J. Heeger, *Science*, 1995, **270**, 1789–1791.
4 C. J. Brabec, N. S. Sariciftci and J. C. Hummelen, *Adv. Funct. Mater.*, 2001, **11**, 15–26.
5 S. Gunes, H. Neugebauer and N. S. Sariciftci, *Chem. Rev.*, 2007, **107**, 1324–1338.
6 S. E. B. Shaheen, C. J. Sariciftci, N. S. Padinger, F. Fromherz, T. Hummelen and J.C., *Appl. Phys. Lett.*, 2001, **78**, 841–843.
7 G. Li, V. Shrotriya, J. Huang, Y. Yao, T. Moriarty, K. Emery and Y. Yang, *Nat. Mater.*, 2005, **4**, 864–868.
8 G. Dennler, M. C. Scharber and C. J. Brabec, *Adv. Mater.*, 2009, **21**, 1323–1338.
9 A. C. Mayer, S. R. Scully, B. E. Hardin, M. W. Rowell and M. D. McGehee, *Materials Today*, 2007, **10**, 28–33.
10 H. A. Becerril, N. Miyaki, M. L. Tang, R. Mondal, Y.-S. Sun, A. C. Mayer, J. Parmer, M. D. McGehee and Z. Bao, *J. Mater. Chem.*, 2009, **19**, 591–593.
11 R. Mondal, N. Miyaki, H. A. Becerril, J. E. Norton, J. Parmer, A. C. Mayer, M. L. Tang, J.-L. Brédas, M. D. McGehee and Z. Bao, *Chem. Mater.*, 2009, **21**, 3618–3628.
12 M. H. Petersen, O. Hagemann, K. T. Nielsen, M. Jørgensen and F. C. Krebs, *Sol. Energy Mater. Sol. Cells*, 2007, **91**, 996–1009.
13 J. P. Nietfeld, C. L. Heth and S. C. Rasmussen, *Chemical Communications*, 2008, 981–983.
14 B. P. Karsten, L. Viani, J. Gierschner, J. Cornil and R. A. J. Janssen, *J. Phys. Chem. A*, 2008, **112**, 10764–10773.
15 M. Zhang, H. N. Tsao, W. Pisula, C. Yang, A. K. Mishra and K. Mullen, *J. Am. Chem. Soc.*, 2007, **129**, 3472–3473.
16 K. T. Nielsen, K. Bechgaard and F. C. Krebs, *Macromolecules*, 2005, **38**, 658–659.
17 C. Kitamura, S. Tanaka and Y. Yamashita, *Chem. Mater.*, 1996, **8**, 570–578.
18 K. E. S. Phillips, T. J. Katz, S. Jockusch, A. J. Lovinger and N. J. Turro, *J. Am. Chem. Soc.*, 2001, **123**, 11899–11907.
19 M. Kozaki, K. Sugimura, H. Ohnishi and K. Okada, *Org. Lett.*, 2006, **8**, 5235–5238.
20 D. Mühlbacher, M. Scharber, M. Morana, Z. Zhu, D. Waller, R. Gaudiana and C. J. Brabec, *Adv. Mater.*, 2006, **18**, 2884–2889.
21 F. Zhang, E. Perzon, X. Wang, W. Mammo, M. R. Andersson and O. Inganäs, *Adv. Funct. Mater.*, 2005, **15**, 745–750.
22 R. S. Ashraf, H. Hoppe, M. Shahid, G. Gobsch, S. Sensfuss and E. Klemm, *Journal of Polymer Science Part A: Polymer Chemistry*, 2006, **44**, 6952–6961.
23 B. S. Nehls, U. Asawapirom, S. Füldner, E. Preis, T. Farrell and U. Scherf, *Adv. Funct. Mater.*, 2004, **14**, 352–356.
24 K. T. Nielsen, K. Bechgaard and F. C. Krebs, *Macromolecules*, 2005, **38**, 658–659.
25 T. Nishi, K. Kanai, Y. Ouchi, M. R. Willis and K. Seki, *Chem. Phys.*, 2006, **325**, 121–128.
26 M. Elstner, D. Porezag, G. Jungnickel, J. Elsner, M. Haugk, T. Frauenheim, S. Suhai and G. Seifert, *Physical Review B*, 1998, **58**, 7260.
27 M. Elstner, P. Hobza, T. Frauenheim, S. Suhai and E. Kaxiras, *Journal of Chemical Physics*, 2001, **114**, 5149.
28 We note that the DFTB approach followed here, while providing a meaningful picture, remains too simple to address the full structural complexity of the polymer films. For instance, even in the case of the dimer packing structures considered here, configurations other than those we presented, such as configurations slightly displaced along the backbone axis, could also exist in the polymer films. A complete analysis of all possible packing structures in the films, based on molecular dynamics / molecular mechanics calculations, is however beyond the scope of this work.
29 R. J. Kline, D. M. DeLongchamp, D. A. Fischer, E. K. Lin, L. J. Richter, M. L. Chabinyc, M. F. Toney, M. Heeney and I. McCulloch, *Macromolecules*, 2007, **40**, 7960–7965.
30 A. C. Mayer, M. F. Toney, S. R. Scully, J. Rivnay, C. J. Brabec, M. Scharber, M. Koppe, M. Heeney, I. McCulloch and M. D. McGehee, *Adv. Funct. Mater.*, 2009, **19**, 1173–1179.
31 F. Zhang, W. Mammo, M. R. Andersson, S. Admassie, M. R. Andersson and O. Inganäs, *Adv. Mater.*, 2006, **18**, 2169–2173.
32 Y. Liang, Y. Wu, D. Feng, S.-T. Tsai, H.-J. Son, G. Li and L. Yu, *J. Am. Chem. Soc.*, 2008, **131**, 56–57.
33 L. J. Lindgren, F. Zhang, M. Andersson, S. Barrau, S. HellstroÌm, W. Mammo, E. Perzon, O. InganaÌs and M. R. Andersson, *Chem. Mater.*, 2009, **21**, 3491–3502.
34 A. P. Zoombelt, M. Fonrodona, M. M. Wienk, A. B. Sieval, J. C. Hummelen and R. A. J. Janssen, *Org. Lett.*, 2009, **11**, 903–906.
35 R. Mondal, S. Ko, J. E. Norton, N. Miyaki, H. A. Becerril, E. Verploegen, M. F. Toney, J.-L. Brédas, M. D. McGehee and Z. Bao, *J. Mater. Chem.*, 2009, **19**, 7195–7197.

